3D Printing with Core-Shell Filaments Containing High- or Low-Density Polyethylene Shells

Fang Peng,[1‡] *Haowei Jiang,*[1‡] *Adam Woods,*[2] *Piljae Joo,*[1] *Eric J. Amis,*[2] *Nicole S. Zacharia,*[1] *Bryan D. Vogt*[1,*]

[1]Department of Polymer Engineering, University of Akron, Akron, OH 44325 USA

[2]Department of Polymer Science, University of Akron, Akron, OH 44325 USA

[‡]These authors contributed equally.

KEYWORDS. Additive manufacturing; fused filament fabrication; FDM; polyolefin; elastic modulus; impact resistance

ABSTRACT

Polyolefins dominate the market for commodity plastics due to their low cost and suitable properties, but polyolefins are rarely used in 3D printing due to issues with deformation of the printed structure during crystallization from the large volume change. Here, we demonstrate that filaments containing approximately 50% of either high density or low density polyethylene (HDPE/LDPE) as a shell with a polycarbonate (PC)/ABS blend core can be printed using standard fused filament fabrication (FFF) methods with adequate to good dimensional accuracy, improved impact resistance, and enhanced elongation at break relative to samples printed with PC/ABS

alone. The combination of lower crystallinity (28 %) of LDPE in comparison to HDPE (62 %) and lower crystallization temperature of LDPE (89 ºC) than HDPE (117 ºC) leads to improved dimensional accuracy of the printed part. However, the elastic modulus of the composite containing LDPE is only 48 % of the part printed with only PC/ABS for flat (XY) orientations, whereas the reduction in modulus with the HDPE shell is significantly less. The mechanical behavior can be rationalized in terms of aligned fiber composite theory where anisotropic modulus is expected to dependent on the angle between stretching direction and fiber axis. The low cost of LDPE and HDPE along with the ability to increase impact strength and extensibility of printed parts further demonstrate the promise of composite core-shell filaments for additive manufacturing.

INTRODUCTION

Additive manufacturing (3D printing) promises new products with massive customization, improved material utilization, and designs incompatible with traditional manufacture.[1-3] Over the past several decades, 3D printing has been used to accelerate prototyping and provide models for improving part designs,[4] but introducing these parts into products has been limited by the inferior and directional mechanical properties of 3D printed parts.[3] For polymers, there are five common classes for 3D printing: extrusion, selective laser sintering, jet printing, sheet lamination, and stereolithography.[3,5] Generally, these printing techniques all build up the part in a layer-by-layer manner, which leads to degradation in mechanical properties from the generation of internal interfaces.[6] There have been some efforts to eliminate these interfaces, particularly by modification of stereolithographic techniques, such as the continuous liquid interface process (CLIP) being commercialized by Carbon.[7] This process can lead to isotropic mechanical properties in 3D printed

polymer parts, but forces generated during printing associated with hydrodynamics can deform the object[8] and there are limitations for adoption due to the high cost associated with specialty photocurable resins. Ideally, low cost commodity thermoplastics could be used in additive manufacturing through fused filament fabrication (FFF),[9] which is a type of extrusion processing for 3D printing. In FFF, the thermoplastic is melted through a hotend and deposited selectively to build a part.[10] However, there are challenges with 3D printing of many commodity plastics, particularly polyolefins, with FFF that arise from the nature of the process.

Due to its relative simplicity, 3D printers based on FFF have infiltrated the consumer market as well as been demonstrated for commercial production, such as the fused deposition modeling (FDM) process from Stratasys.[11] Two polymers, acrylonitrile-butadiene-styrene (ABS)[12] and polylactic acid (PLA),[13] dominate the reports for FFF due to their availability and suitability for 3D printing in terms of adequate mechanical properties and dimensional accuracy. The polymer requirements include that: (1) the filaments are sufficiently stiff to extrude the melt from the hotend of the printer (avoid Euler buckling), (2) the liquification (melt) temperature is within a suitable range for the printer, (3) zero shear melt strength is sufficient to maintain shape as printed, (4) shape is maintained during solidification, and (5) sufficient diffusion occurs across the interface during printing to provide adequate mechanical strength to the 3D printed part. Engineering plastics, such as polycarbonate (PC)[11], polyetherimide (PEI),[14] and poly(ether ether ketone) (PEEK), [13] have been reported but their mechanical properties are only generally slightly better than those for ABS when 3D printed due to challenges in overcoming weaknesses from the interfaces.[13] Despite these requirements, the number of polymers in commercially available filaments for FFF printers has grown significantly in the past several years due to the increased demands for improved performance and functionality of 3D printed parts.

However despite the dominance of polyolefins in terms of the global polymer market and need for recycling of post-consumer polyolefin products,[15] polyolefins only comprise a very small fraction of the commercial filament market with some polypropylene (PP) grades available. For semicrystalline polymers, the volume change on crystallization can lead to warpage of the part from crystallization induced stresses.[16] This large volume provides a challenge for using polyolefins in FFF. For PP, composites have been reported to dramatically decrease the shrinkage (84 %) to help to maintain the printed shape.[17] In general, addition of inorganic fillers can act to improve the dimensional accuracy of 3D printed parts[18,19] by decreasing the coefficient of thermal expansion to decrease stresses developed on cooling and increasing the elastic modulus of the material to reduce the deformation in response to thermal stresses. For polyethylenes (PE), the lower modulus can challenge the initial feeding of the filaments into the printer as the filament can buckle, especially with low density polyethylene (LDPE). There are engineering solutions to enable printing of LDPE by FFF through decreasing the drive-to-nozzle distance and printing at very slow rates.[20] However, this work did demonstrate the potential for additive manufacturing to be local solution to recycling of common plastic waste (LDPE).[20] The decreased modulus of PE in comparison to PP decreases the resistance to warp deformation[21] to adversely affect the dimensional accuracy.

Here we demonstrate the ability to enable enhanced mechanical properties in terms of impact resistance and ductility of 3D printed parts through the inclusion of approximately 50 vol % PE in core-shell filaments where a high-performance PC/ABS blend was used as the core material and the control polymer for comparisons. This large PE content could act to significantly decrease the cost of filaments for FFF. Both LDPE and high-density PE (HDPE) were examined as shell materials. The higher crystallinity of the HDPE (62 %) than the LDPE (28 %) leads to a smaller decrease in the elastic modulus in comparison to the neat PC/ABS, but increased warp

deformation. The impact resistance is more than doubled with the core-shell filaments in comparison to the neat PC/ABS, but these do not quite achieve the impact resistance associated with much higher cost engineering plastics in core-shell filaments (PC and Surlyn).[22] Additionally, the failure mechanism of the parts under tensile load changes from brittle fracture for the 3D printed PC/ABS to ductile for the core-shell materials. These results demonstrate that core-shell filaments provide a potential route to use low cost polyolefins in FFF 3D printing with improvements in the impact properties and extension prior to failure of the parts.

EXPERIMENTAL SECTION

Materials and Filament Manufacture. Commercial polycarbonate/Acrylonitrile-Butadiene-Styrene (PC/ABS) copolymer blend (Bayblend T45PG, Covestro LLC), high density polyethylene (HDPE, SUNTEC B161, ASAHI KASEI) and low-density polyethylene (LDPE, ADSYL 5C37F, Lyondellbasell) were used as the polymers for the fabrication of 3D-printing filaments. Prior to extrusion to fabricate the filaments or 3D printing of the filaments, the PC/ABS was dried in a vacuum oven for 12 h to remove absorbed water (pellets at 110 °C; filaments at 80 °C). Residual water can lead to severe degradation during melt processing of polycarbonates.[23]

Core-shell filaments were fabricated using two single-screw extruders (Rheomex 252p and Akron Extruder M-PAK 150), both of which are equipped with a separate gear pump, that are connected to the core-shell co-extrusion die with a circular opening (diameter = 2 mm). A schematic for this process is shown in Figure 1A. Details about this co-extrusion system have been reported elsewhere.[22] Table 1 shows the temperature profiles used for the extrusion of the different filaments. These temperatures are within the acceptable processing window per the manufacturer's datasheets for the polymers examined here. Both extruders have 3 separate heating zones and a melt pump, which provides 4

independently controlled temperatures. The extruded filaments were quenched in a room-temperature water bath and wound onto a take-up wheel. The speed of the take-up wheel was used to draw the diameter of the extruded filaments down to 1.70 ± 0.03 mm. This drawing of the filaments also acts to improve the uniformity of the filament diameter, which is an important factor in the mechanical properties obtained from 3D printing with FFF.[24]

Table 1. Temperature profiles in the extruders for fabrication of the filaments

Filament		Zone 1 (°C)	Zone 2 (°)	Zone 3 (°C)	Gear Pump (°C)	Die (°C)
PC/ABS		220	230	240	240	230
PC/ABS@LDPE	core	220	230	240	240	200
	shell	170	180	190	190	
PC/ABS@HDPE	core	220	230	240	240	200
	shell	170	180	190	190	

Characterization of Polymers and Filaments. The thermal properties of the as-received, filament extruded, and 3D printed polymers were determined by differential scanning calorimetry (TA Instruments DSC, Model Q50). To assess the crystallinity of polyethylene content in co-extruded filaments and 3D printed samples, polyethylene shells were mechanically stripped from PC/ABS@LDPE and PC/ABS@HDPE core-shell filaments, and thin (0.2-0.4 mm) sections were cut from the corresponding 3D-printed tensile samples and ultrasonicated in Dimethylformamide (DMF) for 1 h to remove all of the PC/ABS without impacting the PE. The samples (4-6 mg) were sealed in hermetic aluminum pans and heated at 10°C min^{-1} under a nitrogen atmosphere from room

temperature to 240 °C to determine the crystallinity of the PE. The properties of the neat polymers on cooling at 10°C min^{-1} under a nitrogen atmosphere from 240 °C to 0 °C were also measured to determine the solidification temperatures (T_c and T_g). The composition of the core-shell filaments was confirmed by quantification of the cross-section of the filaments using optical microscopy (Olympus BX51). To prepare the cross-sections, the filaments were sealed in epoxy resins and cut into 0.1 mm sections using a LECO VC-50 Precision Diamond Cutter.

3D printing of filaments. The fabricated filaments were used with a Cartesio 3D printer (model: W09) equipped with an E3D-v6 (1.75 mm type) hot-end (liquefier) to print impact bars (ASTM-D256) and tensile dogbones (ASTM-D638V). The hot-end was heated with a 24 V–40 W cartridge heater (E3D) and the nozzle had a diameter of 0.4 mm. The extrusion temperature (T_{ext}) was varied between 260 °C and 300 °C as the extrusion temperature tends to affect both the mechanical properties and dimensional accuracy. The print platform was heated to 120 °C and covered first with Kapton tape and then a thin layer of washable poly(vinyl alcohol) adhesive (Elmer's glue stick). The combination of Kapton and poly(vinyl alcohol) was found to promote adhesion of the core-shell polymers to the print platform. The thickness of each layer was set to 0.21 mm. The first layer was printed at an extrusion speed of 10 mm/s in order to ensure good contact with the platform stage to maintain the shape of the part. The other layers were printed at 20 mm/s. All samples were built in a 0°/90° infill pattern with a theoretical 100% infill density. After the build, the part was rinsed liberally with DI water to remove any residual PVA adhesive.

Two orientations were examined for the printing of the impact bars: flat (XY) and edge on (XZ). The schematics for these orientations are shown in Figure S1. The impact bar dimensions matched ASTM-D256, 63.5 mm (length) × 12.7 mm (width) × 4 mm (thick). For sample printed in XZ direction, a 4 mm-wide brim extended from the edge of the sample was printed to the first layer to

provide more surface area for the printed object to stick onto the print platform. For the tensile tests, samples were printed in the XY (flat) orientation with a total thickness of 1.5 mm in accordance with ASTM-D638V at the same temperatures as the impact samples.

Dimensional/Structural Characterization. A 3D scanner (GOM Metrology, ATOS Core 200) was used to determine the shape of the printed sample. The dimensional accuracy of the printed part was elucidated by direct comparison to the computer (CAD) model. In order to obtain highly accurate measurements of the printed objects, the specimens were first coated with white primer (RUST-OLEUM) and decorated with multiple reference points. The number and location of the reference points were selected to ensure that at least 3 reference points were captured in each image. In each image, all individual measurements scans are automatically transformed into a common coordinate system with a complete 3D point cloud. In order ensure that the sample remained stationary during the measurement, the sample was fixed in clay. Since the clay will cover part of the sample at the base, each sample was scanned twice to combine mesh models into one single 3D mesh model that captures the full printed specimen.

To provide insight into the internal structure of the printed parts, microcomputed x-ray tomography (μCT, Bruker Skyscan1172) operating at 50 kV/200 μA was used. Transmission images were obtained at 0.4° increments over 180° from which the cross section was reconstructed (NRecon). The reconstructed images were imported into a Skyscan CT Analyzer (V1.1) to obtain the full 3D images. The core and shell structure can be resolved in the printed part with μCT due to the differences in the electron density between the PC/ABS core and the LDPE or HDPE shell. Additionally, samples were examined after mechanical testing (both impact and tensile) to provide insights into the failure mechanisms.

Mechanical Testing. Tensile and impact measurements were performed to obtain information about the mechanical properties of the 3D printed samples. An Instron 5567 with a load cell of 1000N was used to measure the tensile properties following ASTM-D638V. These tensile data are reported in terms of engineering stress and strain. The outer cross-section of the tensile gauge section was used to calculate the area for the stress; this area should be similar to the actual cross-section as the porosity of the samples (determined from x-ray tomography) under the print conditions used was small in all cases. The stretching rate was 10 mm/min and all measurements were performed at room temperature. All samples were stretched to failure. The impact properties were obtained using the notched Izod impact resistance test (ASTM D-256). The printed samples were mechanically notched and tapered using a notch cutter (Model TMI 22-05, Testing Machine Inc.). The notch depth was 2.54 mm. The impact resistance of the samples was measured using a standard ASTM D-256 Izod pendulum impact machine (Instron 2950) with 5.5 J pendulum energy.

RESULTS AND DISCUSSION

Figure 1A illustrates the co-extrusion process used to generate the core-shell filaments. Both PC/ABS blend, which comprises the core, and polyethylene (high density and low density), which comprises the shell are melted at elevated temperatures in two separated single-screw extruders with the volumetric output rate of the melts controlled by two gear pumps. The two melt streams merges to form the core-shell structure in the specially designed co-extrusion die. For these studies, the volume fraction of the core in the co-extruded filaments was controlled to be 50% by matching the volumetric output rate of the two gear pumps. This composition has been confirmed by optical microscopy on the cross-sectioned filament (Figure S3). The volume fractions calculated from the cross-sections are 46.7 % LDPE and 47% HDPE for the two core-shell filaments. We have previously demonstrated the efficacy of this core-shell approach with filaments containing

approximately 50-50 of the core-shell to improve the impact properties of 3D printed parts,[22] but only for a single system with expensive polymers for both the core and shell.

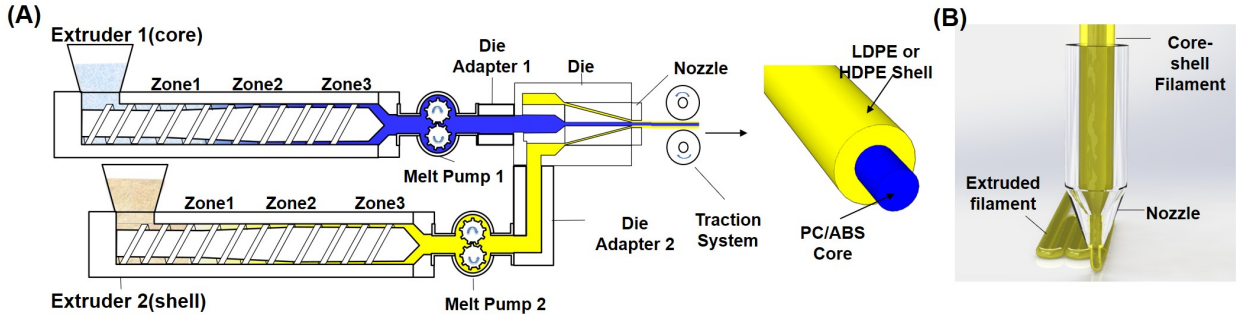

Figure 1. (A) Schematic of coextrusion process to fabricate PC/ABS@LDPE or PC/ABS@HDPE core-shell filaments. (B) Schematic 3D printing core-shell filaments by fused filament fabrication (FFF).

Figure 1B schematically illustrates how the core-shell filaments are used in the FFF 3D-printing process, which is essentially unchanged from traditional filaments in terms of processing but the printed part maintains the core-shell structure internally.[22] During the 3D-printing, the core-shell filament is continuously fed into a temperature-controlled nozzle (often referred to as the liquefier), in which the solid filament is melted and then deposited onto a build-platform through the nozzle orifice. Here the extrusion temperature for 3D-printing of core-shell materials was between 260 °C to 300 °C, which is high enough to melt both the core (T_g of PC/ABS = 140 °C) and shells (T_m of LDPE = 90 °C and HDPE = 110 °C). Lower extrusion temperatures led to challenges in the smooth extrusion of the PC/ABS, while yellowing occurred at temperatures higher than 300 °C. A conformal shell layer appears to remain around the core through the nozzle as the core distribution in the printed part is uniform. When the melt filament is deposited onto the platform, adjacent printed filaments are bonded together through chain diffusion between the shells.[25] Increased chain diffusion should act to improve the weld line interface between printed

filaments, but this is balanced by the adhesion strength between the core and shell polymer. LDPE and HDPE crystallize (T_c) at 89 °C and 117 °C respectively as shown in Figure 2. These temperatures are lower than the glass transition temperature (T_g= 127°C, Figure 2) of the PC/ABS core. The lower solidification temperature of the PE shell in comparison to the PC/ABS core should enable the PE to diffuse over a broader temperature range during cooling in comparison to the PC/ABS. For PE alone, the diffusion should not be appreciably affected under the same print conditions as the thermal conductivity of the polymers are similar, but the dimensional accuracy would be adversely impacted by the volume change on crystallization of the whole printed bead. This enhanced diffusion in comparison to neat PC/ABS filaments along with crystallization of chains across the interface could act to improve the strength of the interface between printed filaments. The mechanical properties of FFF manufactured parts are known to be highly anisotropic due to the weak point at the filament interfaces.[12,26] Therefore, to examine the mechanical properties of 3D-printed parts, impact test specimens were printed with flat (XY) and edge-on (XZ) orientations; these orientations are schematically illustrated in Figure S1.

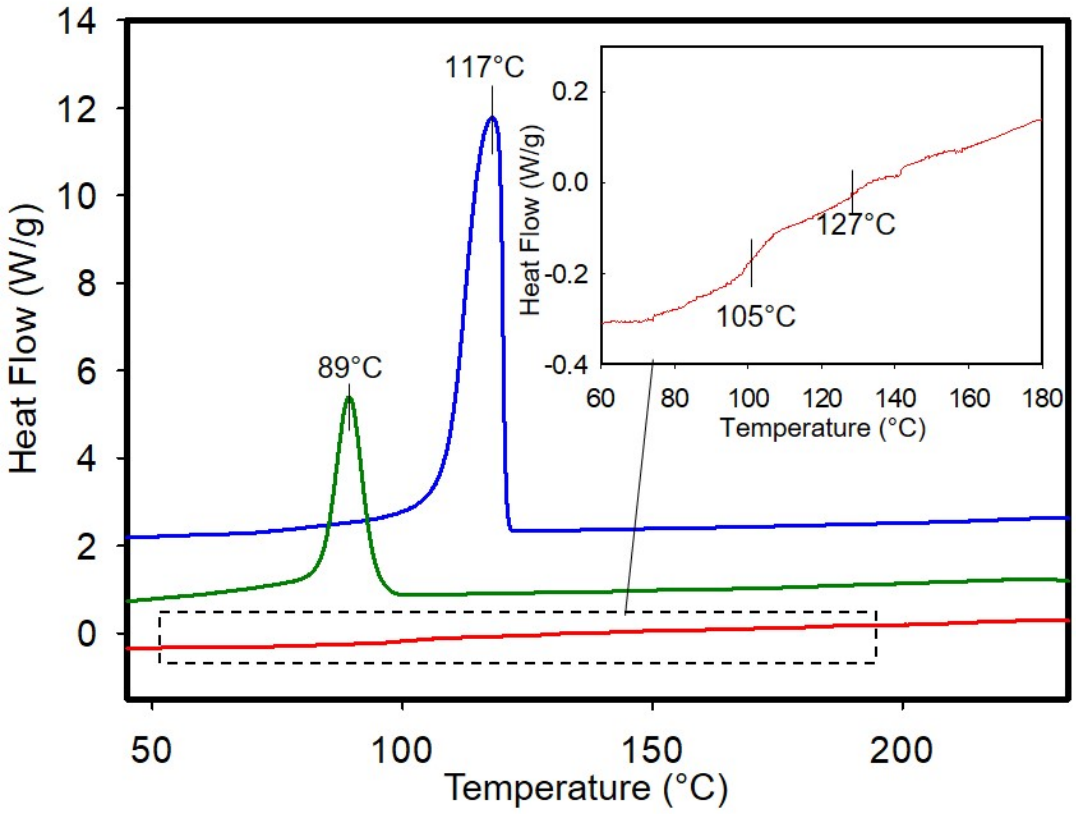

Figure 2. DSC thermograms for the different components of the filaments on cooling at 10°C/min. The polymers were heated first to 240 °C to remove their thermal history prior to the DSC measurements during cooling. The crystallization temperatures for HDPE and LDPE as well as the glass transition temperatures for the PC/ABS blend (see inset for a smaller range to better illustrate T_gs) are determined from the thermograms.

Application of polyethylene filaments in FFF 3D-printing are limited by the warpage deformation due to their significant volume shrinkage on crystallization. Unlike the other semi-crystalline thermoplastics that are widely used in FFF such as PLA[27] or Polyamide[27], the high crystallinity of the HDPE (62%, see Figure S4) used in this study would generally lead to unacceptable shrinkage induced internal stress on crystallization. Due to the abrupt density change during crystallization, warpage deformation has been a common challenge, even for traditional

molding of polyethylene.[28] These same stresses lead to significant warpage deformation in the layer-by-layer printing process of HDPE filament, and more catastrophically, delamination of the part from the build-platform during the print process. The delamination leads to failure during the printing of impact specimens with filaments of only HDPE (as shown in Figure S5). On the other hand, due to its low modulus, LDPE filaments cannot withstand the stress applied in FFF extrusion process, which leads to buckling. Therefore, LDPE is generally unable to be printed alone, although with a sufficiently slow print rate and short drive-to-nozzle distance LDPE can be printed by FFF.[20] In contrast to these semicrystalline olefins, PC/ABS is a partially miscible polymer blend that is widely used in electrical devices and automobile interiors due to their combination of good mechanical and thermal properties associated with PC and easy processability and good notched impact resistance associated with ABS.[29,30] The incorporation of the PC/ABS as the core polymer provides sufficient stiffness to withstand the force during extrusion without buckling even with a LDPE shell. Similarly, the PC-ABS core allows HDPE to be printed without severe warpage deformation.

Figure 3 shows the false color images of impact test specimen that are printed in XZ direction at different extrusion temperatures. The color scale illustrates the local dimensional deviation from the original CAD model in the 3D-scanning image at the surface of the samples. As shown in the left column in Figure 3, specimen printed with pure PC/ABS filament replicates the original CAD model with only minor deviation near the outer edges of the sample printed at 260 °C, but the surface roughness significantly increases at higher printing temperature (280 °C and 300 °C), which is associated with the red and gray colors in the images. The increased roughness of the PC/ABS printed at high temperature is likely to be associated with the lower viscosity of the polymer at higher temperature and the associated flow at the sample edges. The

center column in Figure 3 shows that the rectangular-shaped specimens printed with PC/ABS@LDPE core-shell filaments provide improved dimensional accuracy as compared to those printed with pure PC/ABS. This comparison indicates the ability of LDPE shell to generate a smoother finish of FFF printed samples at high temperature. The right column in Figure 3 shows that impact samples printed with the PC/ABS@HDPE core-shell filaments are rectangular and mostly free from the severe shrinkage-induced warpage deformation that is observed during printing of pure HDPE (Figure S5). Although there is substantial shrinkage with PC/ABS@HDPE filaments in comparison to PC/ABS@LDPE or PC/ABS, the PC/ABS core effectively mitigates the shrinkage-induced deformation of HDPE.

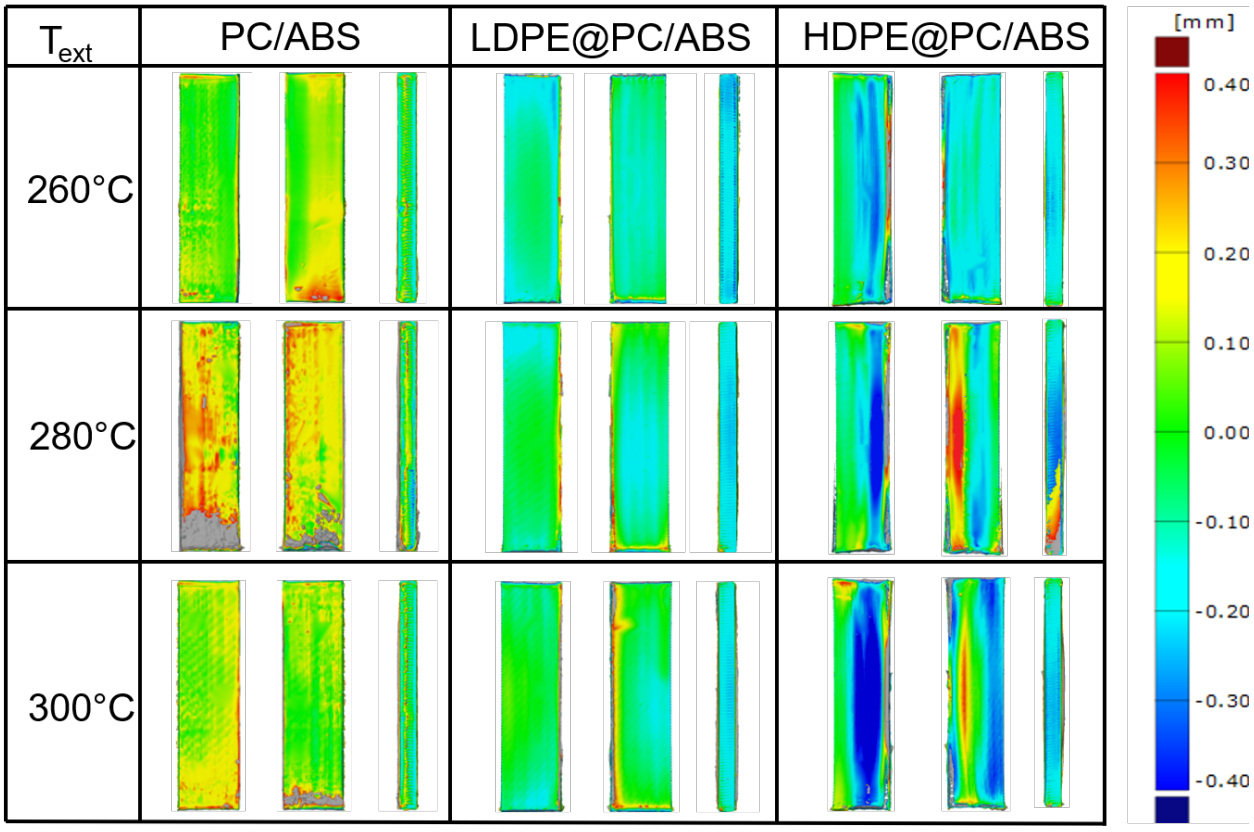

Figure 3. 2D representations of the impact bars [63.5 mm (length) × 12.7 mm (width) × 4 mm (thick)] from the front, back and side (left to right) when printed in the XZ direction at different

extrusion temperature as determined from 3D scanning. The color scale corresponds to dimensional deviation (<0.4 mm) from the CAD design for printing with red representing excessive material on the surface and blue representing insufficient filling of material in comparison to the part design.

Figure 4 illustrates how the impact resistance of these 3D printed samples depends on the composition of the filaments, extrusion print conditions, and the print orientation. It should be noted that the PC/ABS blend is known for its superior notched impact resistance in comparison to most other materials used in FFF. The notched impact resistance of 3D printed PC/ABS is less than 200 J/m, which is much lower than the commonly reported value from injection molded specimens (406 J/m at 23°C, equivalent to 40kJ/m^2 impact strength).[31] The large decrease in impact resistance for 3D printed objects as compared to injection molded ones is attributed to the poor strength of the interfaces between printed filament and associated void content in the printed samples. As shown in Figure 4, PC/ABS@PE core shell filaments significantly increase the impact resistance in both XY and XZ orientations, irrespective of the extrusion temperatures. The data from the impact test are included in Table S1. The impact resistance of PC/ABS@LDPE samples and PC/ABS@HDPE samples printed in XZ orientation decreases as the printing extrusion temperature increases, but these are still significantly greater than neat PC/ABS. The possible cause of decreased mechanical properties at high temperature is the more active thermal degradation at increased temperature[32,33]. Figure 4A shows that the impact resistance is enhanced more with the HDPE shell when printed in XZ direction, whereas the impact resistance improvement is greater for the PC/ABS@LDPE samples printed in XY direction (Figure 4B). HDPE is known to be less impact-resistant as compared to LDPE[31] or PC/ABS blend[29,30]. Therefore, the impact resistances shown in Figure 4 indicate that a toughening mechanism distinct from the

combination of the bulk properties of core and shell is responsible for the increased impact resistance with the PC/ABS@HDPE printed parts.

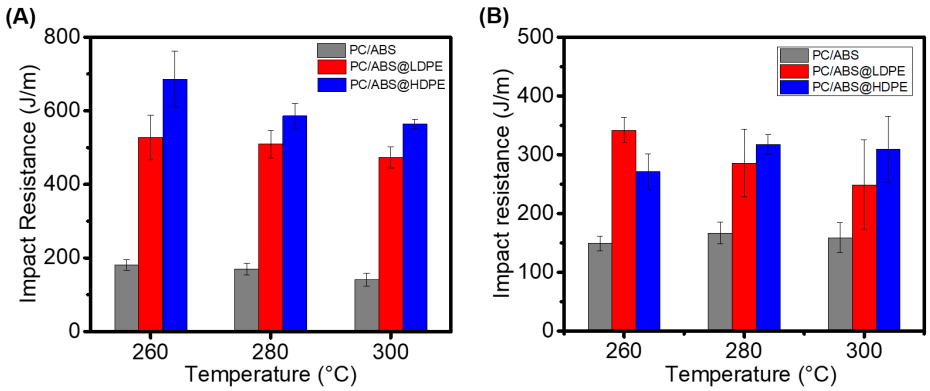

Figure 4. Impact resistance of 3D printed samples of PC/ABS, LDPE-PC/ABS and HDPE-PC/ABS materials when printed in the (A) XZ and (B) XY directions at 260, 280 and 300 °C.

To investigate the origins of the enhanced impact properties, X-ray microCT was used to assess the morphology after impact. Figure 5A illustrates the structure of the damage zone after impact for a specimen printed in the XZ geometry with PC/ABS@LDPE. A crack is generated starting from the notch, but the crack only propagates about 60% of the way through the thickness of the specimen. In the damage zone, fibers of PC/ABS bridges across the crack as shown in the cross-section image of the damage zone in Figure 5A. In addition, core-shell delamination observed near the end of the crack indicates that the impact energy generates a crack through LDPE matrix whereas the delaminated PC/ABS core fibers bridging the cracked zone are not cracked. The smaller cross-section of delaminated fibers as compared to the fibers in the LDPE matrix suggests the delaminated fibers are stretched by the impact energy.

Figure 5B illustrates the structures in the PC/ABS@HDPE samples after impact. The reduced distance of the crack propagation suggests that most of the impact energy is dissipated through mechanisms other than crack propagation for the PC/ABS@HDPE. The cross-section image

shown in Figure 5B demonstrate cracks transverse to the impact direction at the core-shell interface. These minor cracks could act to dissipate part of the impact energy. Because the PC/ABS core and PE shell are immiscible thermoplastics, the core-shell interface in the printed parts is the weakest point in the final part as opposed to the weld line interface between each printed filament, which is commonly the weak link in additively manufactured parts with FFF.[26,35,36] The debonding between core and shell not only provide an additional energy dissipation mechanism in the printed samples, but also limits the crack propagation to prevent the core from failing. Examination of the fibers bridging across the interface (Figure 5A) demonstrates a decreased diameter for the single fibers of the PC/ABS. This change in dimension is consistent with stretching deformation of the PC/ABS fibers that bridge the cracks. This plastic deformation could act to dissipate impact energy. The stretching of the PC/ABS cores appears to be significantly reduced with the HDPE matric (Figure 5B) as the diameter of the PC/ABS fibers that bridge the crack are generally similar to the size in the intact regions. Additionally, the samples overall appear to compress and buckle during the impact test from examination of the cross-sections of both core-shell specimens (Figure 5A and 5B) where the edge opposite to the impact is deformed from the original shape. The inhibition of simple crack propagation through the sample enables large scale (global) deformation upon impact instead of only local crack generation and propagation. From examination of the damage zone, the energy dissipation mechanisms to toughen the samples printed with core-shell samples were identified as core-shell debonding, stretching deformation of the core, crack inhibition, and sample bending.

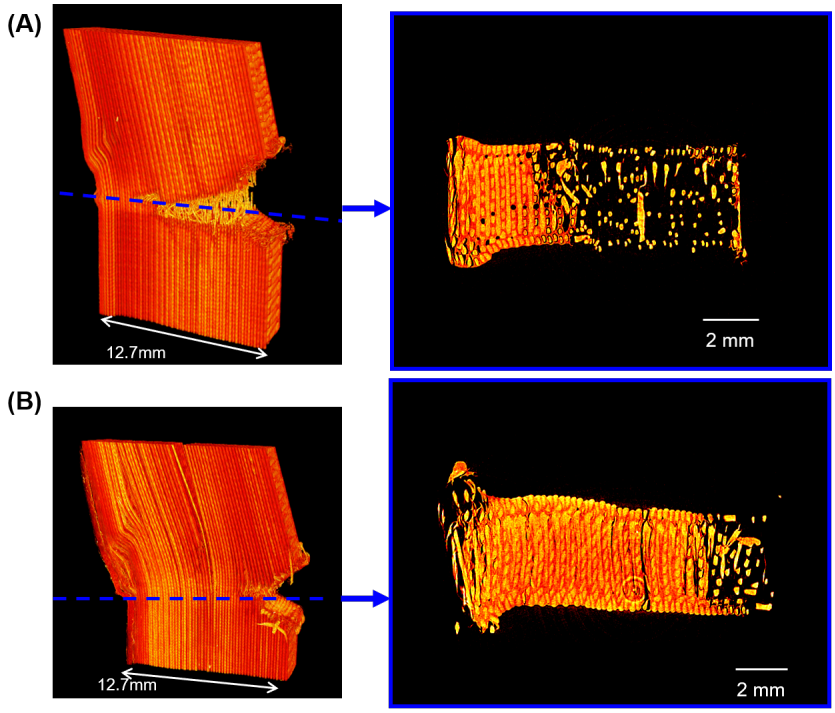

Figure 5. X-ray μCT characterization of impact bars printed in the XZ direction after Izod impact test with (left) 3D side-view (left) and (right) cross-section images for (A) PC/ABS@LDPE and (B) PC/ABS@HDPE. The cross-section is showed at the center of the notch as marked by the blue dashed line. The yellow regions are PC/ABS core and darker red regions are associated with the LDPE or HDPE due to the differences in density between the polymers.

Although the core-shell approach leads to significant improvements in impact properties, it is critical to understand the tensile properties as these are important for any application of the printed parts. With the different geometry of tensile bars in comparison to the impact bars, examination of the dimensional accuracy can provide insights into how the part geometry may impact the ability to obtain a high-quality part. As shown in Figure 6, the dimensional deviation in comparison to the digital model for the tensile bars is similar to what was observed previously for the impact bars (Figure 3). At low temperatures, surface roughness for parts printed with pure PC/ABS samples can be clearly observed. These lines are mostly eliminated at the highest temperature examined, but the tensile bar is

thinner than the digital model in the neck (light blue in middle image), but wider at the bottom (red in the right image). These differences are consistent with the PC/ABS flowing under gravity during the print due to the high temperature. For the core-shell filaments, the surface finish appears improved at all temperatures, but there is warpage deformation after removal from the build-platform. This warpage is most prominent for extrusion at 300 °C, which is likely due to the high temperature softening the PC/ABS domains to decrease their efficacy in holding the shape. The warpage was most severe with the PC/ABS@LDPE. However, decreasing the temperature to 280°C significantly decreases the warpage of the tensile bars with the core-shell filaments. At these lower temperatures, the warpage is greater for the PS/ABS@HDPE as would be expected based on the higher overall crystallinity and higher T_c of HDPE than that for LDPE (Figure 2). When the core-shell filaments are extruded at 280 °C, the shape accuracy of the tensile bars is best, similar to the findings for the impact bars.

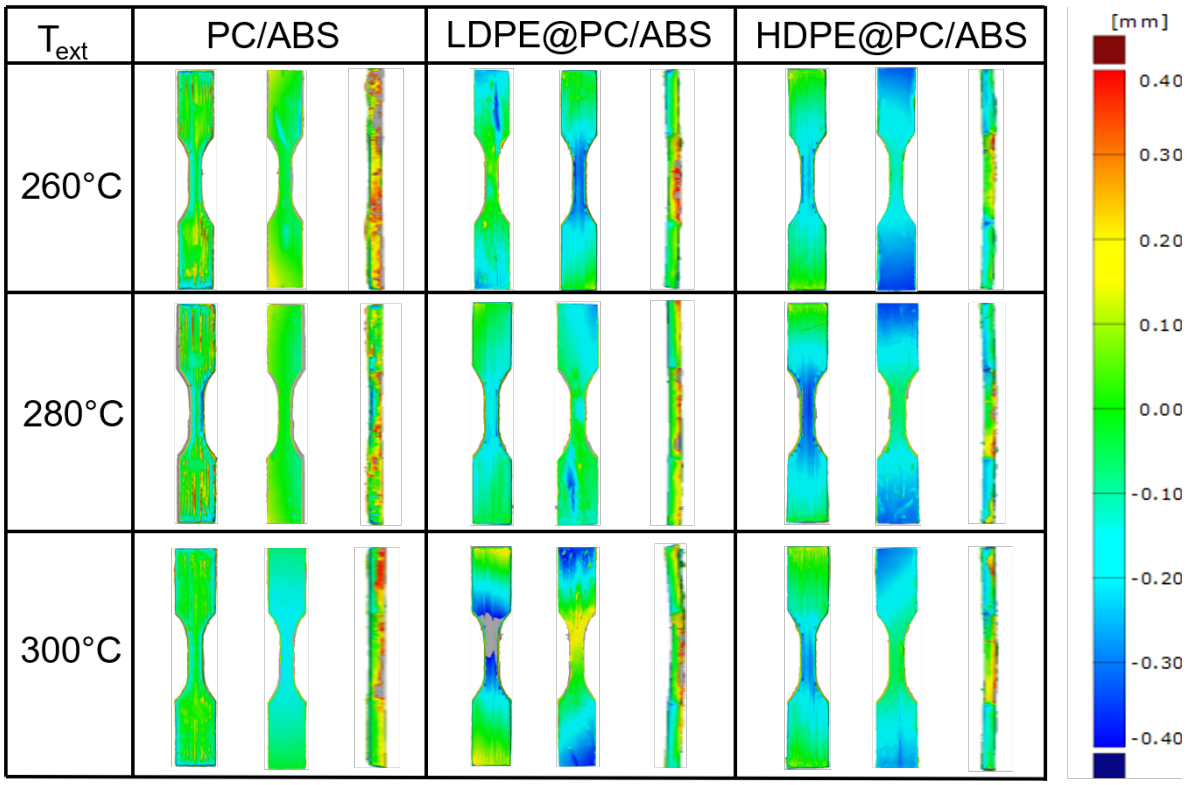

Figure 6. Determining the dimensional accuracy of the 3D printed tensile bar (ASTM-D638V) through 3D-scanning. The images show different sides of tensile samples (top, bottom and side) printed in XY direction at different extrusion temperature. The color scale corresponds to dimensional deviation (< 0.4 mm) from the CAD design.

Figure 7A shows the stress–strain curves for the tensile tests on samples printed at 280°C. Additional stress-strain curves for the other printing conditions are shown in Figure S7. The PC/ABS sample fails immediately after yielding, which suggests a brittle fracture mode. This is counter to the reported ductile tensile behavior of compression molded PC/ABS.[37] This decrease in ductility is commonly observed[38–40] for 3D-printed samples due to their poor weld-line interface strength and higher void defect concentration than with traditional manufacturing. Conversely, the samples printed with core-shell samples do not fail directly after yielding. Instead for the core-shell materials, the tensile stress decreases in a stepwise manner as the strain increases beyond the

yield strain. This behavior is similar to the stepwise failure mode for fiber reinforced composites.[38,39] Each drop in tensile stress is attributed to the tensile failure of an individual fiber in the composite.[39] The composite-like tensile properties is consistent with the internal structures of the samples printed with core-shell samples, in which the polyethylene matrix filled with continuous PC/ABS fibers oriented along X- and Z- axis as shown in Figure S6. From the tensile data (Figure 7A), mechanical properties of the printed parts were determined. Figure 7B shows how the elastic modulus decreases for the core-shell parts in comparison to the 3D-printed PC/ABS. This decrease in modulus is expected because LDPE (473 MPa) and HDPE (1080 MPa) are intrinsically less stiff than the PC/ABS blend (2659 MPa) when processed by compression molding. It is important to note that the modulus of 3D-printed PC/ABS is approximately half of the modulus obtained from compression molding of the same PC/ABS due to weak points at the weld-line interface. The core-shell filaments containing 50 % of either LDPE or HDPE, but the elastic moduli of their 3D printed parts are reduced by much less than the weighted average based on the compression molded properties. A larger difference between the neat PC/ABS and the core-shell materials is found for the yield stress (Figure 7C). This decrease in yield stress can be explained in terms of the lower intrinsic modulus of the polyethylenes. However, the toughness as determined from the area under the stress-strain curves is significantly enhanced by the ductility of the samples printed with the core-shell filaments (Figure 7D). This result is consistent with the increased impact resistance as determined from the notched Izod impact tests (Figure 4). However, the improvement in toughness determined from the tensile measurements (Figure 7D) is significantly greater than the improvement in toughness determined from impact properties (Figure 4). The larger improvement in toughness can be attributed to the slow strain rate of tensile test in comparison to the Izod impact test, which allows more uniaxial stretching deformation of PC/ABS core fibers the PE matrix to

dissipate more energy during the test. Overall, these tensile data show that there is a trade-off associated with the inclusion of polyethylene in the filaments due to the poorer intrinsic mechanical properties of LDPE and HDPE in comparison to the PC/ABS.

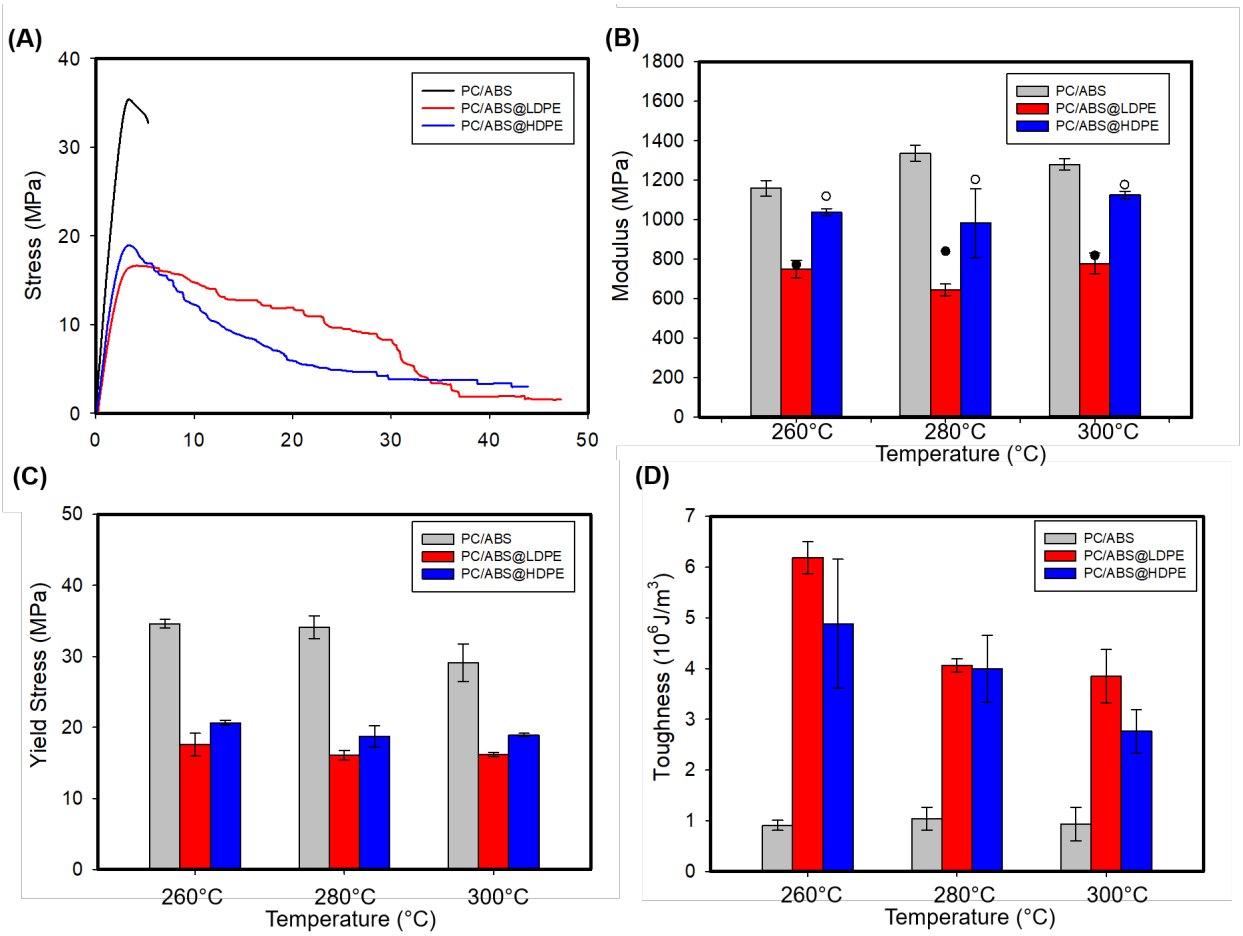

Figure 7. Tensile properties for the 3D-printed PC/ABS, PC/ABS@LDPE and PC/ABS@HDPE materials. (A) Stress-strain curves of parts printed at 280°C. (B) Dependence of processing conditions and composition of the filament on the Young's modulus of the printed part. Composite theory can be used to estimate the modulus for the core-shell samples for (●) LDPE and (○) HDPE shells. (C) The yield stress is significantly reduced with the core-shell filaments due to the lower intrinsic properties of the polyethylenes, but (D) toughness of 3D printed parts determined from

the area under the stress-strain curve is substantially improved with the core-shell filaments irrespective of printing temperature.

To understand the failure mode of the core-shell samples, the fracture areas were examined using X-ray microCT after the tensile tests. Figure 8A illustrates the fracture surface of a PC/ABS@LDPE sample. Similar to the impact bars, PC/ABS fibers are extended from the fracture surface. The thicknesses of these exposed fibers are different from the original structure (Figure S6) with a broader distribution of thicknesses after failure, which we attribute to the PC/ABS fibers being extended and breaking at different elongation at break to change the draw on the fiber. These changes in the structure are consistent with stepwise failure of individual fibers during stretching that was hypothesized from the behavior of the stress-strain curves. The cross-section image (Figure 8B) illustrates core-shell delamination at the fracture surfaces during tensile test, similar to the failure observed from impact. The different cross-section shapes of the delaminated fibers suggest that the step-wise failure modes of the fibers begin with core-shell delamination, because the fibers that remain in contact with the LDPE matrix have a more uniform cross-section shape and are not exposed at the fracture surface. A similar structure is observed after tensile failure for the PC/ABS@HDPE materials (Figure 8C and 8D). Unlike for impact, the damage structure is not obviously different between the HDPE and LDPE.

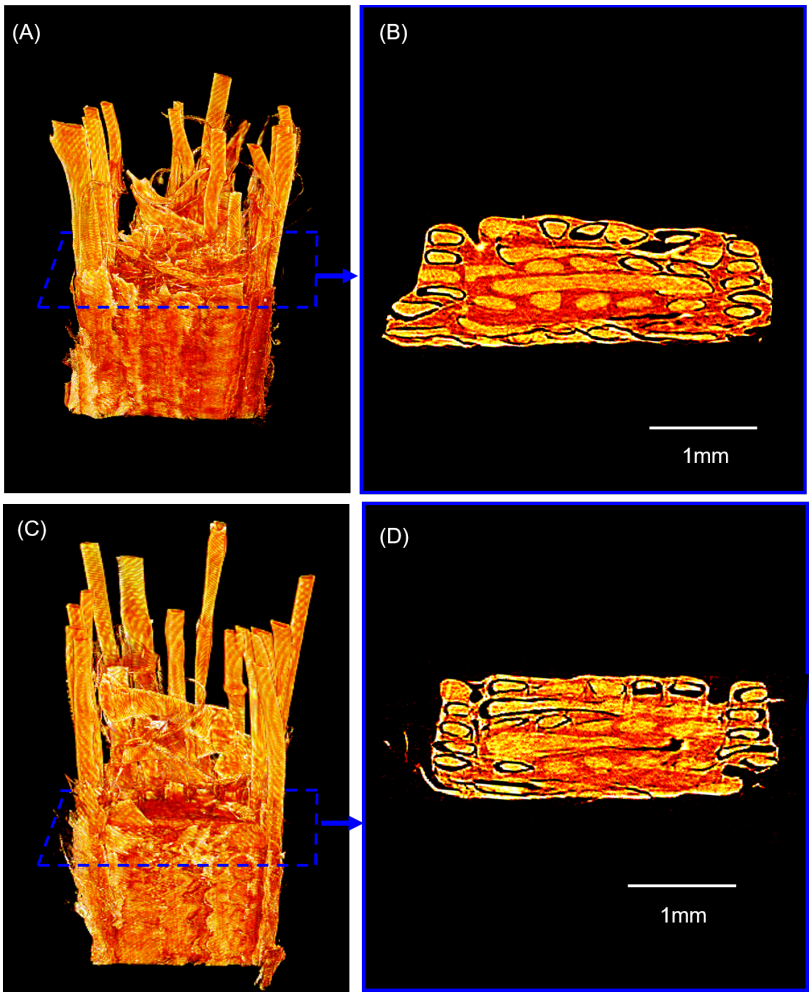

Figure 8. Structure of damage zone determined from X-ray μCT of PC/ABS@LDPE with (A) 3D images and (B) fracture surface at location marked in A of 3D printed tensile specimen printed in the XY direction. Analogous images for PC/ABS@HPDE are shown in C and D. The PC/ABS is shown in red, while the LDPE and HDPE are yellow regions in the X-ray μCT images.

Examination of the internal structures and tensile behavior of the samples printed using the core-shell filaments demonstrates the potential for their mechanical properties to be described in terms of models developed for fiber reinforced polymer composites with defined layups. Here we use a model that was developed for describing the elastic modulus of continuous fiber reinforced

composites by Jaquect *et al*.[43] to predict the elastic properties of the samples printed with the core-shell materials. For the tensile samples, there are 7 layers of deposited filaments with a layup orientation that alternates between 0° and 90° relative to the primary axis of the tensile bar (elongation direction). We can calculate the expected modulus of the layers with the 0° orientation (E_0) as shown in equation (1) and similarly the modulus of layer printed with 90° orientation (E_{90}) from equation (2) based on the rule of mixtures for a unidirectional fiber-reinforced composite.[43]

$$\mathrm{E}_0 = \mathrm{E}_{\mathrm{core}} f_{\mathrm{core}} + \mathrm{E}_{\mathrm{shell}} \left(1 - f_{\mathrm{core}}\right) \tag{1}$$

$$\mathrm{E}_{90} = \frac{\mathrm{E}_{\mathrm{core}}\mathrm{E}_{\mathrm{shell}}}{\mathrm{E}_{\mathrm{shell}} + \mathrm{E}_{\mathrm{core}}\left(1 - \sqrt{f_{\mathrm{core}}}\right)/\sqrt{f_{\mathrm{core}}}} + + \mathrm{E}_{\mathrm{shell}}\left(1 - \sqrt{f_{\mathrm{core}}}\right) \tag{2}$$

where $\mathrm{E}_{\mathrm{core}}$ and $\mathrm{E}_{\mathrm{shell}}$ are the moduli of the core (fiber) and shell (matrix) materials and f_{core} is the volume fraction of the core polymer in the filaments, which based on the conservation of mass will be equal to the composition of the printed part. As the printed tensile bars contain 4 layers oriented at 0°(n_0=4) and 3 layers oriented at 90° (n_{90}=3), the expected elastic modulus of the printed core-shell filament materials is:

$$\mathrm{E} = \mathrm{E}_0 \, {}^{\mathrm{n}_0}\!/_{(\mathrm{n}_0 + \mathrm{n}_{90})} + \mathrm{E}_{\mathrm{shell}} \, {}^{\mathrm{n}_{90}}\!/_{(\mathrm{n}_0 + \mathrm{n}_{90})} \tag{3}$$

Using the elastic modulus of the 3D-printed PC/ABS as E_{core}, while $\mathrm{E}_{\mathrm{shell-HDPE}} = 1080$ MPa and $\mathrm{E}_{\mathrm{shell-LDPE}} = 473$ MPa were obtained from compression molded samples due to the inability to 3D print these neat polymers, the estimated moduli of core-shell 3D printed samples are $\mathrm{E}_{\mathrm{PC/ABS@HDPE}} = 1178$ MPa and $\mathrm{E}_{\mathrm{PC/ABS@LDPE}} = 819$ MPa. These predicted moduli agree quite well with the measured elastic moduli of the 3D printed core-shell parts (Figure 7B). This agreement is consistent with our hypothesis that the printed core-shell materials behave as oriented

fiber composites. As properties from compression molded PE materials are used in this calculation, this suggests that the PE shells can act to increase of the strength of weld line interfaces between adjacent printed filaments in 3D-printed objects to achieve mechanical properties closer to those expected from traditional polymer processes. It should be noted that the strength of the weld interface will be dependent on the rheological characteristics[6] of the PE and thus the efficacy of the PE shell could change if different PE is used. The correspondence of the mechanical behavior to oriented fiber composites also provides potential insights into the role of the strength of the interface between the core and shell on the properties as this should correspond to the matrix-filler interface for composites, which has been extensively studied.[44]

These core-shell filaments based on polyethylene provide several new insights into the design of structured filaments for use in FFF 3D printing. The large difference in solidification temperature between the core and shell used with the initial reports (~90 °C)[22] is not necessary to achieve high impact resistance for the printed part as the T_g of the PC/ABS and the T_c of the HDPE are within 10 °C (Figure 2), but the impact properties are significantly enhanced with the core-shell architecture (Figure 4). The temperature offset between the core and shell appears to be more critical to obtaining good dimensional accuracy. Within a narrow processing window, the warpage of the PC/ABS@HDPE can be controlled to a reasonable level, but small deviations lead to significant increases in the warpage or other deformations that adversely impact the dimensional accuracy. The larger difference in solidification temperature between PC/ABS and LDPE (Figure 2) appears to be correlated with a decreased warpage when printed away from the optimal conditions. An even larger processing window in terms of good dimensional accuracy for the PC@Surlyn core-shell filaments previously reported, which has the largest difference between the core and shell. This decreased sensitivity to the processing variability with these core-shell

filaments when there is a large difference in the solidification temperature of the core and shell may prove useful to improve the part yield for additive manufacturing with FFF.

CONCLUSION

In this work, we demonstrate the ability to effectively include polyethylene (PE) thermoplastics in 3D printing by FFF through the use of co-extruded filaments where the shell of the filament is PE. Here PC/ABS@PE core–shell filaments containing ≈50 vol% PE overcome the poor stiffness and shrinkage induced shape inaccuracy of LDPE and HDPE; these properties have historically limited the application of PE as FFF feedstock. These core-shell filaments lead to 3D printed parts with significantly enhanced toughness when compared with the PC/ABS alone. The failure of the 3D printed parts transitions from brittle failure for PC/ABS to ductile with the core-shell filaments. The core–shell filament yields a composite-like architecture where the continuous PC/ABS fibers along X- and Y- axis act as reinforcement. The immiscibility of PC/ABS and PE leads to debonding under modest stresses, which provides a mechanism to increase stretching of PC/ABS fibers to dissipate energy for enhanced toughness. Although the tensile properties are reduced in comparison to PC/ABS, the tensile performance of the PC/ABS@PE objects conforms to expectations from fiber reinforced composite due to the intrinsic lower modulus of PE. The reduced window to solidify the core of the filament prior to crystallization with HDPE along with its higher overall crystallinity tends to lead to increased warpage of the printed samples. The difference in the warpage between HDPE and LDPE cores indicates that the crystallinity and the differences in the solidification temperature between the core and shell impact the dimensional accuracy of the 3D printed part. These results illustrate the potential for using polyethylene in 3D printing to overcome the brittle and failure prone nature of standard 3D-printed parts.

ASSOCIATED CONTENT

Supporting Information.

The following files are available free of charge.

Schematic of 3D printing orientations, images of coextruded filaments, DSC data for determining crystallinity, image of warpage delamination with HDPE, x-ray tomography images of the internal structure of core-shell printed parts, tabulated impact data, and tensile stress-strain curves. (PDF)

AUTHOR INFORMATION

Corresponding Author

* To whom correspondence should be addressed: vogt@uakron.edu (B.D.V.)

Author Contributions

The manuscript was written through contributions of all authors. All authors have given approval to the final version of the manuscript. ‡These authors contributed equally.

ACKNOWLEDGMENTS

This work was financially supported by the Division of Civil, Mechanical and Manufacturing Innovation (CMMI) in the Directorate for Engineering of the National Science Foundation, grant CMMI- 1825276. The authors thank Covestro LLC (Pittsburgh, PA) for donation of the PC/ABS, Asahi Kasei for donation of the HDPE and Lyondellbasell for donation of the LDPE.

REFERENCES

(1) Biswas, K.; Rose, J.; Eikevik, L.; Guerguis, M.; Enquist, P.; Lee, B.; Love, L.; Green, J.; Jackson, R. Additive Manufacturing Integrated Energy—Enabling Innovative Solutions for Buildings of the Future. *J. Sol. Energy Eng.* **2017**, *139*, 15001.

(2) Tofail, S. A. M.; Koumoulos, E. P.; Bandyopadhyay, A.; Bose, S.; O'Donoghue, L.; Charitidis, C. Additive Manufacturing: Scientific and Technological Challenges, Market Uptake and Opportunities. *Mater. Today* **2018**, *21*, 22-37.

(3) Ligon, S. C.; Liska, R.; Stampfl, J. J.; Gurr, M.; Mülhaupt, R.; Mülhaupt, R. Polymers for 3D Printing and Customized Additive Manufacturing. *Chem. Rev.* **2017**, *117*, 10212–10290.

(4) Gardan, J. Additive Manufacturing Technologies: State of the Art and Trends. *Int. J. Prod. Res.* **2016**, *54*, 3118–3132.

(5) Stansbury, J. W.; Idacavage, M. J. 3D Printing with Polymers: Challenges among Expanding Options and Opportunities. *Dent. Mater.* **2016**, *32*, 54–64.

(6) Seppala, J. E.; Han, S. H.; Hillgartner, K. E.; Davis, C. S.; Migler, K. B. Weld Formation during Material Extrusion Additive Manufacturing. *Soft Matter* **2017**, *13*, 6761–6769.

(7) Janusziewicz, R.; Tumbleston, J. R.; Quintanilla, A. L.; Mecham, S. J.; DeSimone, J. M. Layerless Fabrication with Continuous Liquid Interface Production. *Proc. Natl. Acad. Sci.* **2016**, *113*, 11703–11708.

(8) Wang, Z.; Liang, H.; Dobrynin, A. V. Computer Simulations of Continuous 3-D Printing. *Macromolecules* **2017**, *50*, 7794–7800.

(9) Turner, B. N.; Gold, S. A. A Review of Melt Extrusion Additive Manufacturing Processes: II. Materials, Dimensional Accuracy, and Surface Roughnessnull. *Rapid Prototyp. J.* **2015**, *21*, 250–261.

(10) Turner, B.N. ; Strong, R.; Gold, S. A. A Review of Melt Extrusion Additive Manufacturing Processes: I. Process Design and Modeling. *Rapid Prototyp. J.* **2014**, *20*, 192–204.

(11) Cicala, G.; Latteri, A.; Del Curto, B.; Lo Russo, A.; Recca, G.; Farè, S. Engineering Thermoplastics for Additive Manufacturing: A Critical Perspective with Experimental Evidence to Support Functional Applications. *J. Appl. Biomater. Funct. Mater.* **2017**, *15*, 10–18.

(12) Ahn, S.-H.; Montero, M.; Odell, D.; Roundy, S.; Wright, P. K. Anisotropic Material Properties of Fused Deposition Modeling ABS. *Rapid Prototyp. J.* **2002**, *8*, 248–257.

(13) Wu, W.; Geng, P.; Li, G.; Zhao, D.; Zhang, H.; Zhao, J. Influence of Layer Thickness and Raster Angle on the Mechanical Properties of 3D-Printed PEEK and a Comparative Mechanical Study between PEEK and ABS. *Materials (Basel).* **2015**, *8*, 5834–5846.

(14) Cicala, G.; Ognibene, G.; Portuesi, S.; Blanco, I.; Rapisarda, M.; Pergolizzi, E.; Recca, G. Comparison of ULTEM 9085 Used in Fused Deposition Modelling (FDM) with Polytherimide Blends. *Materials (Basel).* **2018**, *11*, E285.

(15) Kreiger, M. A.; Mulder, M. L.; Glover, A. G.; Pearce, J. M. Life Cycle Analysis of Distributed Recycling of Post-Consumer High Density Polyethylene for 3-D Printing Filament. *J. Clean. Prod.* **2014**, *70*, 90–96.

(16) Wang, T.-M.; Xi, J.-T.; Jin, Y. A Model Research for Prototype Warp Deformation in the FDM Process. *Int. J. Adv. Manuf. Technol.* **2006**, *33*, 1087–1096.

(17) Stoof, D.; Pickering, K. Sustainable Composite Fused Deposition Modelling Filament Using Recycled Pre-Consumer Polypropylene. *Compos. Part B Eng.* **2018**, *135*, 110–118.

(18) Herrero, M.; Peng, F.; Núñez Carrero, K. Ca.; Merino, J. C.; Vogt, B. D. Renewable Nanocomposites for Additive Manufacturing Using Fused Filament Fabrication. *ACS Sustain. Chem. Eng.* **2018**, *6*, 12393-12402.

(19) Wang, X.; Jiang, M.; Zhou, Z.; Gou, J.; Hui, D. 3D Printing of Polymer Matrix Composites: A Review and Prospective. *Compos. Part B Eng.* **2017**, *110*, 442–458.

(20) Hart, K. R.; Frketic, J. B.; Brown, J. R. Recycling Meal-Ready-to-Eat (MRE) Pouches into Polymer Filament for Material Extrusion Additive Manufacturing. *Addit. Manuf.* **2018**, *21*, 536-43.

(21) Peng, A.; Xiao, X.; Yue, R. Process Parameter Optimization for Fused Deposition Modeling Using Response Surface Methodology Combined with Fuzzy Inference System. *Int. J. Adv. Manuf. Technol.* **2014**, *73*, 87–100.

(22) Peng, F.; Zhao, Z.; Xia, X.; Cakmak, M.; Vogt, B. D. Enhanced Impact Resistance of Three-Dimensional-Printed Parts with Structured Filaments. *ACS Appl. Mater. Interfaces* **2018**, *10*, 16087–16094.

(23) Long, T. S.; Sokol, R. J. Molding Polycarbonate: Moisture Degradation Effect on Physical and Chemical Properties. *Polym. Eng. Sci.* **1974**, *14*, 817–822.

(24) Liu, W. J.; Zhou, J. P.; Ma, Y. M.; Wang, J.; Xu J. Fabrication of PLA Filaments and its Printable Performance. *IOP Conf. Ser.: Mater. Sci. Eng.* **2018**, *275*, 012033.

(25) Coogan, T. J.; Kazmer, D. O. Bond and Part Strength in Fused Deposition Modeling. *Rapid Prototyp. J.* **2017**, *23*, 414-422.

(26) Lee, C. S.; Kim, S. G.; Kim, H. J.; Ahn, S. H. Measurement of Anisotropic Compressive Strength of Rapid Prototyping Parts. *J. Mater. Process. Technol.* **2007**, *187–188*, 627–630.

(27) Wang, L.; Gramlich, W. M.; Gardner, D. J. Improving the Impact Strength of Poly(Lactic Acid) (PLA) in Fused Layer Modeling (FLM). *Polymer (Guildf).* **2017**, *114*, 242–248.

(28) Chen, C. H.; White, J. L.; Ohta, Y. A Fundamental Experimental Study of the Mechanisms of Warpage and Shrinkage of Polyethylene in Rotational Molding. *Int. Polym. Process.* **1991**, *6*, 212–216.

(29) Sorrentino, A. Polycarbonate/ABS Blends: A Literature Review. *Adv. Polym. Technol.* **1994**, *13*, 249–258.

(30) Kerns, J.; Hsieh, A.; Hiltner, A.; Baer, E. Comparison of Irreversible Deformation and Yielding in Microlayers of Polycarbonate with Poly(Methylmethacrylate) and Poly(Styrene-Co-Acrylonitrile). *J. Appl. Polym. Sci.* **2000**, *77*, 1545–1557.

(31) Covestro. Bayblend ® T45 PG Standard Grades / Non Reinforced Bayblend ® T45 PG.

(32) Aboulkas, A.; El harfi, K.; El Bouadili, A. Thermal Degradation Behaviors of Polyethylene and Polypropylene. Part I: Pyrolysis Kinetics and Mechanisms. *Energy Convers. Manag.* **2010**, *51*, 1363–1369.

(33) Park, J. W.; Oh, S. C.; Lee, H. P.; Kim, H. T.; Yoo, K. O. Kinetic Analysis of Thermal Decomposition of Polymer Using a Dynamic Model. *Korean J. Chem. Eng.* **2000**, *17*, 489–496.

(34) Dilara, P. A.; Briassoulis, D. Degradation and Stabilization of Low-Density Polyethylene Films Used as Greenhouse Covering Materials. *J. Agric. Eng. Res.* **2000**, *76*, 309–321.

(35) Sun, Q.; Rizvi, G. M. M.; Bellehumeur, C. T. T.; Gu, P. Effect of Processing Conditions on the Bonding Quality of FDM Polymer Filamentsnull. *Rapid Prototyp. J.* **2008**, *14*, 72–80.

(36) Li, L.; Sun, Q.; Bellehumeur, C.; Gu, P. Investigation of Bond Formation in FDM Process. In *Proc. of Solid Free. Fabr. Sym.;* **2002**, 403, 400–407.

(37) Chiang, W.; Hwung, D. Properties of Polycarbonate/Acrylonitrile-Butadiene- Styrene Blends. *Polym. Eng. Sci.* **1987**, *17*, 632-639.

(38) Bertoldi, M.; Yardimci, M. A.; Pistor, C. M.; Guceri, S. I.; Sala, G. Mechanical Characterization of Parts Processed via Fused Deposition. In *Proc. 1998 Solid Free, Fabr. Sym.*; 1998; pp 557–565.

(39) Rodriguez, J. F.; Thomas, J. P.; Renaud, J. E. Mechanical Behaviour of Acrylonitrile Butadiene Styrene (ABS) Fused Deposition Materials. Experimental Investigation. *Rapid Prototyp. J.* **2001**, *7*, 148–158.

(40) Torrado Perez, A. R.; Roberson, D. A.; Wicker, R. B. Fracture Surface Analysis of 3D-Printed Tensile Specimens of Novel ABS-Based Materials. *J. Fail. Anal. Prev.* **2014**, *14*, 343–353.

(41) Dyer, S. R.; Lassila, L. V. J.; Jokinen, M.; Vallittu, P. K. Effect of Fiber Position and Orientation on Fracture Load of Fiber-Reinforced Composite. *Dent. Mater.* **2004**, *20*, 947–955.

(42) Craig, W. H.; Courtney, T. H. On the Tension Test as a Means of Characterizing Fibre Composite Failure Mode. *J. Mater. Sci.* **1975**, *10*, 1119–1126.

(43) Jacquet, E.; Trivaudey, F.; Varchon, D. Calculation of the Transverse Modulus of a Unidirectional Composite Material and of the Modulus of an Aggregate. Application of the Rule of Mixtures. *Compos. Sci. Technol.* **2000**, *60*, 345–350.

(44) Herrera-Franco, P. J.; Dral, L. T. Comparison of Methods for the Measurement of Fibre/Matrix Adhesion in Composites. *Composites* **1992**, *23*, 2-27.

For TOC only